PERGAMON

International Journal of Rock Mechanics & Mining Sciences 39 (2002) 429–442

International Journal of
Rock Mechanics
and Mining Sciences

www.elsevier.com/locate/ijrmms

A modeling approach for analysis of coupled multiphase fluid flow, heat transfer, and deformation in fractured porous rock

J. Rutqvist*, Y.-S. Wu, C.-F. Tsang, G. Bodvarsson

Earth Sciences Division, Lawrence Berkeley National Laboratory, MS 90-1116, Berkeley, CA 947 20, USA

Accepted 2 February 2002

Abstract

This paper presents the methodology in which two computer codes—TOUGH2 and FLAC3D—are linked and jointly executed for coupled thermal–hydrologic–mechanical (THM) analysis of multiphase fluid flow, heat transfer, and deformation in fractured and porous rock. TOUGH2 is a well-established code for geohydrological analysis with multiphase, multicomponent fluid flow and heat transport, while FLAC3D is a widely used commercial code that is designed for rock and soil mechanics with thermomechanical and hydromechanical interactions. In this study, the codes are sequentially executed and linked through external coupling modules: one that dictates changes in effective stress as a function of multi-phase pore pressure and thermal expansion, and one that corrects porosity, permeability, and capillary pressure for changes in stress. The capability of a linked TOUGH-FLAC simulator is demonstrated on two complex coupled problems related to injection and storage of carbon dioxide in aquifers and to disposal of nuclear waste in unsaturated fractured porous media.

Keywords: Modeling fractured rock coupled deformation fluid flow

1. Introduction

Coupled thermal–hydrologic–mechanical (THM) processes under multiphase flow conditions are prevalent in a number of geoscientific applications [1]. A few of the most important include nuclear waste disposal in geological media, deep underground injection of hazardous waste, geothermal energy extraction, enhanced recovery from oil and gas reservoirs, and underground storage of natural gas. Recently, underground storage of carbon dioxide (CO_2) into permeable aquifers, such as deep saline aquifers, depleted oil and gas reservoirs, and coal seams, has been suggested as an important potential method to reduce the emission of greenhouse gases to the atmosphere [2]. Mathematical modeling of CO_2 injection performance for reservoirs of all kinds must also consider cross-coupling of geochemistry, geomechanics, flow, and transport [3]. Therefore, a coupled THMC (including chemical processes) simulator is required for analysis of these problems of broad international interests. However, except for a few specialized simplified approaches, there is (to the authors' knowledge) no single computer code that handles general coupled THMC processes—including multiphase and multicomponent fluid flow and reactive transport—in geological media.

In this article, as an alternative to developing a single coupled THMC code, two existing well-established codes, each specialized to a few of the above processes, are coupled to potentially cover all four processes (THMC). The two codes—TOUGH2 [4], a THC code, and FLAC3D [5], a THM code—are linked using sequential execution and data transfer through nonlinear coupling functions. The TOUGH2 code solves coupled problems of nonisothermal, multiphase, multicomponent fluid flow in complex geological systems. It has been verified and used by many groups all over the world to study problems in geothermal energy, oil and gas reservoirs, contaminant migration and nuclear waste isolation [6]. Recently, a version of the code (TOUGH-REACT) has been extended for analysis of reactive transport, including precipitation and dissolution of minerals [7]. The FLAC3D code is developed for rock and soil mechanics and can also handle coupled thermomechanical and hydromechanical processes for single-phase fluid flow [8]. Although, in principle, a

*Corresponding author. Tel.: +1-510-486-5432; fax: +1-510-486-5686.

E-mail address: jrutqvist@lbl.gov (J. Rutqvist).

1365-1609/02/$ - see front matter
PII: S1365-1609(02)00022-9

Nomenclature

a	empirical exponent for porosity-stress function (1/Pa)
b, b_m	fracture aperture and "mechanical aperture" (m)
b_i, b_r	initial and residual fracture aperture (m)
b_{max}	maximum mechanical aperture for aperture-normal stress function (m)
c	empirical exponent for porosity-permeability function (dimensionless)
C_s	constant specific heat of solid phase (J/kg K)
d	empirical exponent for aperture versus normal stress function (1/Pa)
D_v	effective molecular diffusion (m^2/s)
e_ψ	specific internal energy per unit mass of phase $\psi = l, g$ (J/kg)
F_ϕ	porosity change factor ($= \phi/\phi_i$) (dimensionless)
F_k	permeability change factor ($= k/k_i$) (dimensionless)
F_{pc}	capillary pressure change factor ($= P_c/P_{ci}$) (dimensionless)
$\mathbf{F_I}$	force vector in node i (N)
$\mathbf{g}$	acceleration of gravity (vector) (m/s^2)
h_ψ^κ	specific enthalpy per unit mass of a component (J/kg)
$\mathbf{i}_\psi^\kappa$	diffusive mass flux of a component in phase $\psi = l, g$ (kg/(m^2 s))
$\mathbf{i}_m^h$	apparent heat conduction over all phases (J/(m^2 s))
$\mathbf{I}$	identity tensor (dimensionless)
$\mathbf{k}$	intrinsic hydraulic permeability tensor (m^2)
K	bulk modulus (Pa)
k, k_0	intrinsic permeability in general and at zero stress (m^2)
k_i	initial intrinsic permeability (m^2)
$k_{r\psi}$	relative permeability for flow in phase $\psi = l, g$ (dimensionless)
M_ψ^κ	mass of component κ per unit volume (kg/m^3)
P_ψ	fluid pressure in phase $\psi = l, g$ (Pa)
P_c	capillary pressure $P_c = P_\ell - P_g$ (Pa)
P	pore fluid pressure in general (Pa)
P^f, P^m	pore fluid pressure in fracture continuum and matrix continuum (Pa)
$\mathbf{q}_\psi^\kappa$	flux density for mass of component κ in phase $\psi = l, g$ (kg/(m^2s))
$\mathbf{q}^h$	flux density for energy over all phases (J/(m^2 s))
Q^κ	source term
s	fracture spacing (m)
S_ψ	saturation of phase $\psi = g, l$ (dimensionless)
t	time (seconds)
T	absolute temperature (K)
$\mathbf{u}$	displacement (vector) (m)
$\mathbf{v}$	solid velocity with respect to a fixed system (m/s)
X_ψ^κ	mass fraction of component κ in phase $\psi = l, g$ (dimensionless)
z	elevation (m)

Greek symbols

α	Biot's constant for a porous media (dimensionless)
α^f, α^m	Biot's constant for fracture system and matrix (dimensionless)
$\beta_{T,}$	linear thermal expansion coefficient of the medium (1/K)
$\boldsymbol{\varepsilon}$	total strain tensor (dimensionless)
ϕ, ϕ^f	porosity in general and porosity of the fracture continuum (dimensionless)
ϕ_0, ϕ_r	porosity at zero stress and residual porosity at infinitely high stress (dimensionless)
ϕ_i	initial porosity (dimensionless)
λ_m	apparent macroscopic thermal conductivity of the rock mass (W/m K)
μ_ψ	dynamic fluid viscosity of fluid phase $\psi = l, g$ (Pa s)
ρ_s	solid mass density (kg/m^3)
ρ_ℓ, ρ_g	liquid and gas density (kg/m^3)
ρ_m	average density of the rock mass (kg/m^3)

$\boldsymbol{\sigma}$	macroscopic total stress tensor (tension positive) (Pa)
$\boldsymbol{\sigma}'$	macroscopic effective stress tensor (tension positive) (Pa)
σ'_{M}	effective all around mean stress ($= 1/3(\sigma'_{x+}\sigma'_y + \sigma'_z)$).
σ'_{n}	effective stress normal across a fracture (tension positive) (Pa)
Special symbols	
$\nabla \cdot \mathbf{A}$	divergence of a vector (=div **A**)
∇A	gradient of a scalar (=grad A)
$\nabla \mathbf{A}$	gradient of a vector
$\times$	scalar multiplication

sequential coupling of two codes is less efficient than having a single code, a big advantage with coupling of TOUGH2 and FLAC3D is that both codes are well tested and widely applied in their respective fields.

This paper describes the method for linking TOUGH2 and FLAC3D for modeling of coupled THM processes in porous and fractured geological media. Although TOUGH2 can model several fluid phases, we are limiting this presentation to two-phase flow (a liquid phase and a gas phase), coupled with heat transfer and mechanical deformations. First, we outline the basic assumptions for simulating a porous, deformable multiphase medium and present the governing equations and numerical procedures of TOUGH2 and FLAC3D. Thereafter, the coupling of the two codes is explained, including approach, coupling functions, and numerical procedure. Finally, two application examples are presented to demonstrate the capabilities of the coupled TOUGH-FLAC simulator.

2. Assumptions for modeling of two-phase flowing porous, deformable geologic media

In the following, a fractured porous rock is treated as a multiphase, nonisothermal, deformable system, where voids of the rock skeleton are filled partially with liquid and partially with gas. Thus, it is a three-phase system (gas, liquid and solid) and each fluid phase may have several components (e.g., water, CO_2, air). The mechanical behavior of the porous and fractured media responds to changes in temperature, and skeletal effective stress and strain. The mechanical responses include changes in porous and fractured media void volumes, with accompanying changes in permeability. Coexisting fluid and solid components are assumed to be in local thermal equilibrium (i.e. locally they are at the same temperature). While a few main fractures may be discretely defined within a rock matrix, the main part of the fractured porous rock is treated as s single continuum or multicontinuum (fracture system and rock matrix). In a multicontinuum model, the temperature and pressure may be different in the matrix and fractures, while the total stress (as opposed to the effective stress) is assumed to be the same in both continua as a requirement for continuity of stress. At least four types of conservation equations are needed to fully describe such a system, including mass balance equations for each fluid components, one energy balance equation, and a momentum conservation equation describing rock deformation forces [9].

3. Governing equations and numerical procedure in TOUGH2

In the formulation for TOUGH2, the total mass balance of each fluid component is accumulated from relevant contributions in each phase ($\psi = g$ for gas and $\psi = l$ for liquid). For a component (e.g., $\kappa = a$ for air, $\kappa = w$ for water, $\kappa = \mathrm{CO_2}$ for CO_2), we obtain

$$\frac{\partial}{\partial t} M^{\kappa} - Q^{\kappa} = -\nabla \cdot (\mathbf{q}_{\ell}^{\kappa} + \mathbf{q}_{g}^{\kappa}), \tag{1}$$

where M^{κ} is the mass per unit volume of component κ computed as

$$M^{\kappa} = \phi S_{\ell} \rho_{\ell} X_{\ell}^{\kappa} + \phi S_{\mathrm{g}} \rho_{\mathrm{g}} X_{\mathrm{g}}^{\kappa}, \tag{2}$$

where ϕ is porosity, S_{ψ} and ρ_{ψ} are saturation and density of phase ψ, and X_{ψ}^{κ} is the mass fraction of component κ in fluid phase ψ.

The mass flux of each component, κ, within each fluid phase, ψ, can be written as the sum of the advective (Darcy) and nonadvective (diffusive) fluxes as:

$$\mathbf{q}_{\psi}^{\kappa} = -\rho_{\psi} X_{\psi}^{\kappa} \frac{\mathbf{k} k_{\mathrm{r}\psi}}{\mu_{\psi}} (\nabla P_{\psi} - \rho_{\psi} \mathbf{g} \nabla z) + \mathbf{i}_{\psi}^{\kappa}, \tag{3}$$

where the diffusive flux is computed (using Fick's law) as

$$\mathbf{i}_{\psi}^{\kappa} = -\rho_{\psi} D_{\mathrm{v}} \mathbf{I} \nabla X_{\psi}^{\kappa} \tag{4}$$

with D_{v} as an effective molecular-diffusion coefficient in a porous media that depends on temperature, gas pressure, medium tortuosity, and gas saturation [10].

Considering all contributions to the heat storage and flux over all phases, the energy conservation equation is assembled as:

$$\frac{\partial}{\partial t}(\phi S_{\ell} \rho_{\ell} e_{\ell} + \phi S_g \rho_g e_g + (1-\phi)\rho_s C_s T) - Q^{\mathrm{h}} = -\nabla \cdot (\mathbf{q}^{\mathrm{h}}), \tag{5}$$

where e_ψ are internal energies of each phase, C_s is specific heat of solid, $\mathbf{q}^h$ is energy flux density (including advective and diffusive fluxes) , and Q^h is the heat source term.

The total heat flux is given by the sum of the advective flux contributions over the fluid phases, and the diffusive flux as

$$\mathbf{q}^h = \sum_\psi \sum_\kappa h_\psi^\kappa \mathbf{q}_\psi^\kappa + \mathbf{i}_m^h, \tag{6}$$

where h_ψ^κ is enthalpy (energy per unit mass) of component κ in phase ψ, and the diffusive or conductive heat conduction is governed by Fourier's law:

$$\mathbf{i}_m^h = -\lambda_m \mathbf{I} \nabla T, \tag{7}$$

where λ_m is the apparent macroscopic (over all phases) thermal conductivity.

In TOUGH2, the continuum equations are discretized in space using the integral finite-difference method [11]. Time is discretized as a first order finite-difference, and a fully implicit scheme is adopted where the fluxes are expressed in terms of the unknown thermodynamic parameters at time level $t^{k+1} = t^k + \Delta t$, leading to the following nonlinear algebraic equations:

$$R_n^{(\kappa)k+1} \equiv M_n^{(\kappa)k+1} - M_n^{(\kappa)k} - \frac{\Delta t}{V_n}\left\{\sum_m A_{nm} q_{nm}^{(\kappa)k+1} + V_n Q_n^{(\kappa)k+1}\right\}, \tag{8}$$

where subscripts n and m label element and element face, R is the residual, M is mass or energy per unit volume (Eq. (2)), V is element volume, A is area of element face, q is flux (Eqs. (3) and (6)) and Q is the source term. The TOUGH2 code performs a complete simultaneous solution of the discretized mass- and energy-balance equations. To handle nonlinearity, a Newton–Raphson iteration scheme is adopted, in which the Jacobian is numerically evaluated for selected primary variables and the solution is achieved when the residual R becomes small.

4. Governing equations and numerical procedure in FLAC3D

When running the FLAC3D code in its mechanical or thermomechanical configuration mode, it solves the equation of motion,

$$\nabla \cdot \boldsymbol{\sigma} + \rho_m \mathbf{g} = \rho_m \frac{d\mathbf{v}}{dt} \tag{9}$$

in an iterative manner with a stress–strain law. The incremental stress and strain during a time step is governed by various elastic or elasto-plastic constitutive laws, which can be written in a general form as

$$\Delta\sigma' = \mathbf{H}(\sigma', \dot{\varepsilon}\Delta t) \tag{10}$$

in which $\mathbf{H}$ contains given material functions, $\dot{\varepsilon}$ is the infinitesimal strain-rate tensor, and Δt is a time increment. Eq. (10) is valid for small strain, but in the FLAC3D code a large strain formulation can be invoked, in which the stress tensor is corrected for rotational strains.

The infinitesimal strain rate, $\dot{\varepsilon}$, and infinitesimal strain, $\boldsymbol{\varepsilon}$, is governed by the restrictions

$$\dot{\varepsilon} = \frac{1}{2}(\nabla \mathbf{v} + (\nabla \mathbf{v})^{tr}) \qquad \varepsilon = \frac{1}{2}(\nabla \mathbf{u} + (\nabla \mathbf{u})^{tr}), \tag{11}$$

where tr denotes the transpose of a tensor. As usual, the total strain increment can be decomposed into elastic, plastic, and thermal expansion parts, according to:

$$\Delta\varepsilon = \Delta\varepsilon^e + \Delta\varepsilon^p + \Delta\varepsilon^T, \tag{12}$$

where the thermal strain is given by

$$\Delta\boldsymbol{\varepsilon}^T = \mathbf{I}\beta\Delta T \tag{13}$$

and where β_T is the linear thermal expansion coefficient, $\mathbf{I}$ is the unit tensor and T is temperature.

The constitutive laws in Eq. (10) work on the effective stress, which can be calculated (by invoking the FLAC3D groundwater configuration) as:

$$\boldsymbol{\sigma}' = \boldsymbol{\sigma} + \mathbf{I}\alpha P, \tag{14}$$

where α is Biot's effective stress parameter [12] and P is pore pressure.

In FLAC3D, the continuum equations are discretized in space using a first order finite difference technique and special mixed discretization approach. In this approach, the finite difference equations are derived using constant strain-rate elements of tetrahedral shapes, which are then overlaid to form final zone elements. The overlaying technique is necessary to provide more modes of deformations during plastic flow. Time derivatives are discretized using an explicit finite difference formulation, leading to the following form of the equation of motion:

$$\mathbf{v}_i^{(t+\Delta t/2)} = \mathbf{v}_i^{(t-\Delta t/2)} + \frac{\Delta t}{m}\sum_i \mathbf{F}_i^t, \tag{15}$$

where $\mathbf{v}$ indicates nodal velocities, m is the lumped nodal mass, and $\mathbf{F}$ is nodal force. In FLAC3D, the basic explicit dynamic calculation iterates between solving the equation of motion and the stress–strain constitutive equation using a sufficiently small time step to assure numerical stability. In one time step, the equation of motion is first invoked to calculate new velocities based on previous velocities and forces. The nodal velocities are then used to derive new strain rates and stress, which in turn are used to update the force vector of Eq. (15). The final solution is reached (using a damped solution) when the body is in equilibrium or in steady-state flow (plastic flow), and the out of balance force goes to zero.

5. Coupling of TOUGH2 and FLAC3D

When linking two codes, the coupled equations cannot be solved simultaneously; they should be solved sequentially, with coupling parameters passed to each equation at specific intervals. Therefore, in this study, the TOUGH2 and FLAC3D codes are executed sequentially on compatible numerical grids (Fig. 1) and linked through external coupling modules, which serve to pass relevant information between the field equations that are solved in respective code.

5.1. Hydromechanical coupling approach

The approach taken here is to couple TOUGH2 and FLAC3D through the concept of effective stress or modified effective stress and nonlinear empirical expressions for changes in hydraulic properties as a function of effective stress. These empirical functions could be estimated from laboratory data and should if possible be determined by model calibration against field experiments at a relevant scale. The coupling functions take into account the most essential couplings including effects of rock deformation on porosity, permeability and capillary pressure, and the effects of fluid pressure and temperature on rock deformation. Using this approach, the governing equations presented for each code in Sections 3 and 4 are essentially unchanged and solved sequentially within respective code. However, for the case of a rapidly changing effective stress (relative to fluid mobility), the mass balance Eq. (1) can be corrected with an additional term as:

$$\frac{\partial}{\partial t}M^{\kappa} + M^{\kappa}\alpha\frac{\partial \varepsilon_v}{\partial t} - Q^{\kappa} = -\nabla\cdot(\mathbf{q}^{\kappa}_{r\ell} + \mathbf{q}^{\kappa}_{rg}), \tag{16}$$

where ε_v is volumetric strain and subscript r on the flux terms indicates mass flux relative to the solid phase. Eq. (16) takes into account the movement of fluid relative to the rock and the movement of the rock relative to a fixed control volume [9]. The expression is approximate in the sense that some smaller terms for the effect of grain compressibility have been neglected and small strain is assumed.

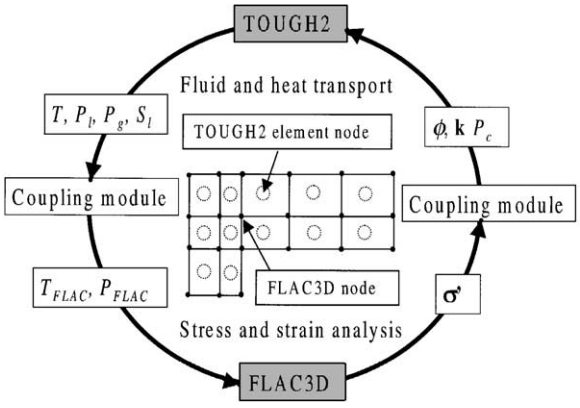

Fig. 1. Schematic of linking TOUGH2 and FLAC3D for a coupled THM simulation.

5.2. TOUGH-FLAC coupling modules

A TH to M link takes multiphase pressures, saturation, and temperature from the TOUGH2 simulation and provides updated temperature, and pore pressure to FLAC3D (Fig. 1). Because a TOUGH2 mesh uses one gridpoint within each element, and FLAC3D nodes are located in element corners, data have to be interpolated from mid-element (TOUGH2) to corner locations (FLAC3D). After data transfer, FLAC3D internally calculates thermal expansion and effective stress according to Eqs. (13) and (14), with the thermal expansion and effective-stress coefficients given in the FLAC3D input deck. A coupling module for this link essentially performs the interpolation from TOUGH2 to FLAC3D nodes and calculates an average pore pressure in FLAC3D nodes, based on a material-specific effective stress law.

An M to TH link takes element stress or deformation from FLA3D and corrects element porosity, permeability, and capillary pressure for TOUGH2. In TOUGH2, the newly updated hydraulic properties for each element are entered into the fluid and heat flow calculation through Eq. 8. In addition, the effects of volumetric strain in Eq. (16) can be entered into Eq. (8) as an extra contribution to the source term. No interpolation in space is required for this data transfer because stress and strain are defined in FLAC3D elements, which are identical to TOUGH2 elements. A TOUGH-FLAC coupling module for this link should calculate the hydraulic property changes, based on material-specific theoretical or empirical functions.

5.3. TOUGH-FLAC numerical procedure

A separate batch program can control the coupling and execution of TOUGH2 and FLAC3D for the linked TOUGH-FLAC simulator. In this case, it was done within the FLAC3D input file using the FLAC-FISH programming language [5]. The calculation is stepped forward in time with the transient TH analysis in TOUGH2, and at each time step or at the TOUGH2 Newton iteration level, a quasi-static mechanical analysis is conduced with FLAC3D to calculate stress-induced changes in porosity and intrinsic permeability. The resulting THM analysis may be explicit sequential, meaning that the porosity and permeability is evaluated only at the beginning of each time step, or the analysis may be implicit sequential, with permeability and porosity updated on the Newton iteration level towards the end of the time step using an iterative process.

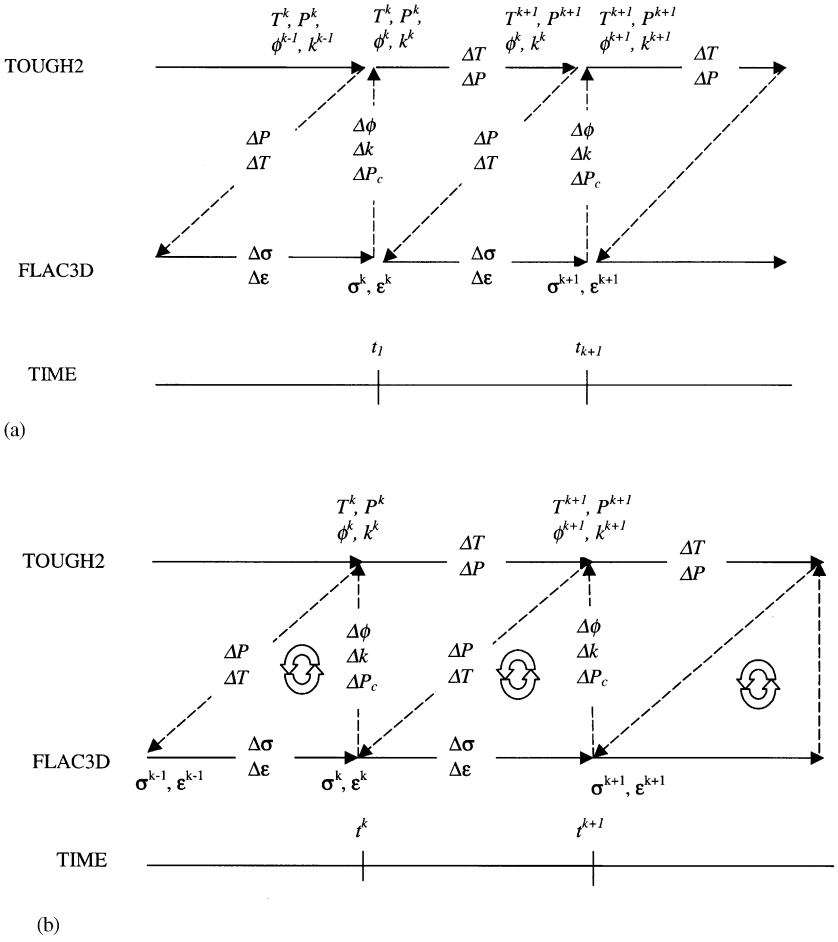

Fig. 2. Numerical procedure of a linked TOUGH2 and FLAC3D simulation with (a) explicit sequential and (b) implicit sequential solutions.

In the explicit sequential procedure (Fig. 2a), the TOUGH2 code is executed for a TH analysis between time t^k to t^{k+1} until mass conservation is assured by solving Eq. (8). During this time step, the porosity and permeability are assumed to be constant, according to the values evaluated at the beginning of a time step. The mass term, $M_n^{(\kappa)k}$ in Eq. (8), represents the conditions at the end of the previous time step and should therefore include the previous porosity ϕ^k. On the other hand, the mass term $M_n^{(\kappa)k+1}$ and the flux term $F_n^{(\kappa)k+1}$ should include the new porosity ϕ^{k+1} and the new permeability k^{k+1}, which were evaluated at the beginning of the time step.

In the implicit sequential procedure (Fig. 2b), porosity and permeability are updated with every Newton iteration (within each time step) of the TOUGH2 Newton–Raphson scheme. Thus, at mass balance, the resulting permeability and porosity are evaluated at the end of the time step, which then is transferred smoothly to the next time level.

The explicit sequential scheme requires less computation effort because each code is executed only once in each time step, which also implies that data is only transferred once in each time step. The explicit sequential solution should be accurate if the porosity and permeability varies slowly with time or if time step size relatively small. For example, when modeling coupled THM processes around a nuclear waste repository, it is expected that slowly evolving thermal strains cause most changes in porosity and permeability. On the other hand, when modeling problems with significant strain rate and "hydraulic squeezing", time steps must be limited for an accurate solution. When using the implicit sequential scheme there is no time limitations for accuracy, however, large time steps may induce numerical stability problems.

6. Coupling relationships for linked TOUGH-FLAC simulations

In this section, we are presenting empirical hydro-mechanical coupling relationships for applications in two types of rocks: porous sedimentary aquifer rock and

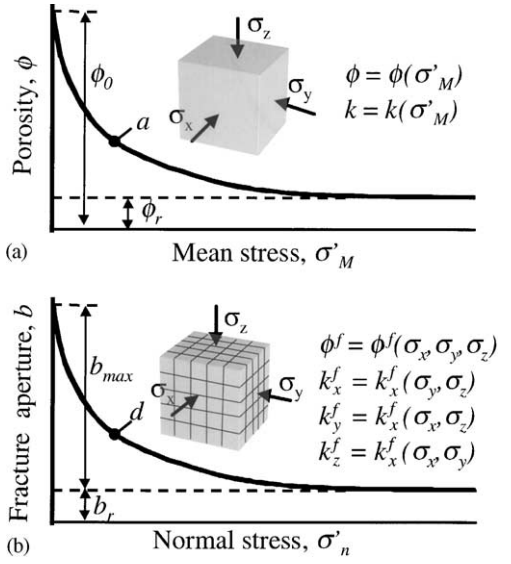

Fig. 3. Conceptual models and basic nonlinear coupling functions for (a) porous sedimentary aquifer rock and (b) highly fractured volcanic tuff.

highly fractured porous hard rock. These functions are developed for applications two application examples presented in Section 7: sequestration of CO_2 greenhouse gas in a brine aquifer and a high temperature nuclear waste repository in unsaturated and fractured rock. The functions for highly fractured rock are developed for volcanic tuff at a potential site for a nuclear waste repository, Yucca Mountain, Nevada. In this model, the fracture and matrix flow and their interaction are modeled using a dual-permeability (overlapping continuum) concept. Figs. 3a and b illustrates the two model conceptualizations for correcting the hydraulic properties with stress. The nonlinear coupling functions are empirical and should be calibrated against site-specific data for an accurate representation.

6.1. Effective stress function for porous sedimentary rock

For unsaturated porous media, an average fluid pressure—which depends on both liquid and gas pressure—replaces the fluid pressure in Eq. (14). By taking the volume average of the pressure in the two fluids, we can derive following average pore pressure [13]:

$$P = S_\ell P_\ell + (1 - S_\ell) P_g. \tag{17}$$

Other weights in determining P leads to a different equation. If for example S_ℓ is replaced with an experimentally determined Bishop's factor [14], a Bishop's type of modified effective stress law is obtained.

6.2. Effective stress function for a highly fractured hard rock

In a multicontinuum structure, the average fluid pressure in each continuum could be calculated according to Eq. (17). Furthermore, the factor αP in Eq. (14) could be replaced by the following theoretical expression [15]:

$$\alpha P = \alpha^{\mathrm{f}} P^{\mathrm{f}} + \alpha^{\mathrm{m}} P^{\mathrm{m}}, \tag{18}$$

where P^{f} and P^{m} are calculated according to Eq. (17) and α^{f} and α^{m} are effective stress constants for the fracture system and matrix respectively. Restrictions on the values of α^{f} and α^{m} are given by Chen et al. [15]. The coefficients α^{f} and α^{m} can be estimated from laboratory measurements according to Walsh [16] and Iwano [17], which both suggested that α^{f} could be considerable less than unity. However, for fractured hard rocks in the unsaturated zone, the changes in pore pressure are generally small—the gas pressure is near atmospheric and the liquid pressure similar to the capillary pressure—and may not induce any significant deformations in the fractured rock system. Thus, in the unsaturated zone, the impact of fluid pressure on the mechanics may be negligible.

6.3. Correction of hydraulic properties of porous sedimentary rock

For the porous sedimentary rock the isotropic hydraulic properties are corrected using empirical porosity-mean stress and permeability-porosity relationships that can be fitted to laboratory experiments on sandstone by Davis and Davis [18]. The porosity, ϕ, is related to the mean effective stress, σ'_{M} as

$$\phi = \phi_{\mathrm{r}} + (\phi_0 - \phi_{\mathrm{r}}) \exp(a \times \sigma'_{\mathrm{M}}), \tag{19}$$

where ϕ_0 is porosity at zero stress, ϕ_r is residual porosity at high stress, and the exponent a should be experimentally determined (Fig. 3a).

The permeability is correlated to the porosity according to the following exponential function (modified from Davis and Davis, [18]):

$$k = k_0 \exp[c \times (\phi/\phi_0 - 1)], \tag{20}$$

where k_0 is permeability at zero stress and the exponent c should be experimentally determined.

In addition to the two coupling functions in Eqs. (19) and (20), the capillary pressure is modified with permeability and porosity according to a function by Leverett [19]:

$$P_{\mathrm{c}} = P_{\mathrm{c0}}(S_\ell) \frac{\sqrt{k_0/\phi_0}}{\sqrt{k/\phi}}. \tag{21}$$

Thus, porosity, permeability and capillary pressure are all directly or indirectly dependent on the mean stress.

6.4. Correction of hydraulic properties of a highly fractured hard rock

For a highly fractured dual-permeability medium, we only present coupling functions for the fractured continuum, whereas the matrix properties could be related to the mean stress similar to the functions presented in Section 6.3. However, in fractured hard rock, stress-induced changes in hydraulic properties are expected to be much greater in compliant rock fractures than in the stiffer matrix. To correct rock mass permeability for a change in the three-dimensional stress field, a cubic-block conceptual model is utilized (Fig. 3b). Using this model, the porosity, permeability, and capillary pressure in the fractured continuum is corrected for any change in the stress field according to:

$$\phi^{\mathrm{f}} = F^{\mathrm{f}}_{\phi} \times \phi^{\mathrm{f}}_{\mathrm{i}}, \tag{22}$$

$$k^{\mathrm{f}}_{x} = F^{\mathrm{f}}_{kx} \times k^{\mathrm{f}}_{x\mathrm{i}}, \quad k^{\mathrm{f}}_{y} = F^{\mathrm{f}}_{ky} \times k^{\mathrm{f}}_{y\mathrm{i}}, \quad k^{\mathrm{f}}_{z} = F^{\mathrm{f}}_{kz} \times k^{\mathrm{f}}_{z\mathrm{i}}, \tag{23}$$

$$P^{\mathrm{f}}_{\mathrm{c}} = F^{\mathrm{f}}_{\mathrm{Pc}} \times P^{\mathrm{f}}_{\mathrm{ci}} \tag{24}$$

where F are correction factors, subscript i denotes initial conditions, and superscript f denotes "fracture continuum".

The porosity and permeability correction factors are calculated from the initial and current apertures in fracture set 1, 2, and 3 according to:

$$F^{\mathrm{f}}_{\phi} = \frac{b_1 + b_2 + b_3}{b_{1\mathrm{i}} + b_{2\mathrm{i}} + b_{3\mathrm{i}}}, \tag{25}$$

$$F^{\mathrm{f}}_{kx} = \frac{b_2^3 + b_3^3}{b_{2\mathrm{i}}^3 + b_{3\mathrm{i}}^3}, \quad F^{\mathrm{f}}_{ky} = \frac{b_1^3 + b_3^3}{b_{1\mathrm{i}}^3 + b_{3\mathrm{i}}^3}, \quad F^{\mathrm{f}}_{kz} = \frac{b_1^3 + b_2^3}{b_{1\mathrm{i}}^3 + b_{2\mathrm{i}}^3}, \tag{26}$$

where fractures in fracture sets 1, 2, and 3 are assumed to be equally spaced and oriented normal to x, y, and z axes, respectively, and a parallel plate fracture flow model [20] is adopted. The current fracture aperture b depends on the current effective normal stress, σ'_{n}, according to the following exponential function [21]:

$$b = b_{\mathrm{r}} + b_{\mathrm{m}} = b_{\mathrm{r}} + b_{\max}[\exp(d \times \sigma'_{\mathrm{n}})], \tag{27}$$

where b_{r} is a residual aperture, b_{m} is "mechanical" aperture, $b_{\max}$ is the maximum "mechanical" aperture and d is a parameter related to the curvature of the function (Fig. 3b). This relationship can also be expressed in terms of an initial aperture, b_{i} and changes in aperture, Δb as:

$$b = b_{\mathrm{i}} + \Delta b = b_{\mathrm{i}} + b_{\max}[\exp(d \times \sigma'_{\mathrm{n}}) - \exp(d \times \sigma'_{\mathrm{ni}})], \tag{28}$$

where σ_{ni} is the initial stress normal to the fractures. This expression can be inserted into Eq. (26) to derive expressions for permeability correction factors in x, y, and z directions:

$$F^{\mathrm{f}}_{kx} = \frac{[b_{\max}(\exp(d \times \sigma'_{y}) - \exp(d \times \sigma'_{y\mathrm{i}}))]^3 + [b_{\max}(\exp(d \times \sigma'_{z}) - \exp(d \times \sigma'_{z\mathrm{i}}))]^3}{b_{\mathrm{i}2}^3 + b_{\mathrm{i}3}^3}, \tag{29a}$$

$$F^{\mathrm{f}}_{ky} = \frac{[b_{\max}(\exp(d \times \sigma'_{x}) - \exp(d \times \sigma'_{x\mathrm{i}}))]^3 + [b_{\max}(\exp(d \times \sigma'_{z}) - \exp(d \times \sigma'_{z\mathrm{i}}))]^3}{b_{\mathrm{i}1}^3 + b_{\mathrm{i}3}^3}, \tag{29b}$$

$$F^{\mathrm{f}}_{kz} = \frac{[b_{\max}(\exp(d \times \sigma'_{x}) - \exp(d \times \sigma'_{x\mathrm{i}}))]^3 + [b_{\max}(\exp(d \times \sigma'_{y}) - \exp(d \times \sigma'_{y\mathrm{i}}))]^3}{b_{\mathrm{i}1}^3 + b_{\mathrm{i}2}^3}. \tag{29c}$$

The capillary pressure is corrected with porosity and permeability according to the Leverett [19] function:

$$F^{\mathrm{f}}_{\mathrm{Pc}} = \sqrt{\frac{F^{\mathrm{f}}_{k}}{F^{\mathrm{f}}_{\phi}}}, \tag{30}$$

where

$$F^{\mathrm{f}}_{k} = \sqrt[3]{F^{\mathrm{f}}_{kx} \times F^{\mathrm{f}}_{ky} \times F^{\mathrm{f}}_{kz}}. \tag{31}$$

Thus, with these coupling relations, fracture porosity, permeability, and capillary pressure are all directly or indirectly dependent on the three-dimensional stress field, with the possibility of anisotropic permeability changes along the vertical and horizontal directions.

7. Application of TOUGH-FLAC: two examples

Two application examples demonstrate the capability of a TOUGH-FLAC simulator. The first example is related to sequestration of CO_2 greenhouse gas in brine aquifers [22], and the second example is related to a high temperature nuclear waste repository in unsaturated rock [23]. Within each application, the material specific hydromechanical coupling relationships developed in Section 6 are used. In both these applications, the effects of capillary pressure are significant which implies that the pressures of the different fluids are not the same. In the case of CO_2 sequestration, the capillary pressure is important for the sealing mechanism in a caprock above the injection aquifer, and in the case of the unsaturated porous fractured rocks, matrix capillary suction tends to keep the high permeability fractures dry.

7.1. CO_2 sequestration into a brine formation

In this example, the TOUGH-FLAC code is applied to simulate an injection operation for disposal of CO_2 into a permeable brine formation, which is overlain by a semi-permeable caprock (Fig. 4). The injection takes place at a depth of 1500 m so that the CO_2 is within the temperature and pressure range for it to be a super-critical fluid. As a supercritical fluid, the CO_2 behaves like a gas with low viscosity but having a liquid-like density of 200–900 kg/m^3, depending on pressure and temperature. Because the supercritical CO_2 is less dense than water, deep underground disposal requires that the caprock is sufficiently impermeable to trap the injected CO_2 for a sufficiently long time. Important rock-mechanical aspects of this simulation are to study the integrity of the caprock and the possibilities of rock failure.

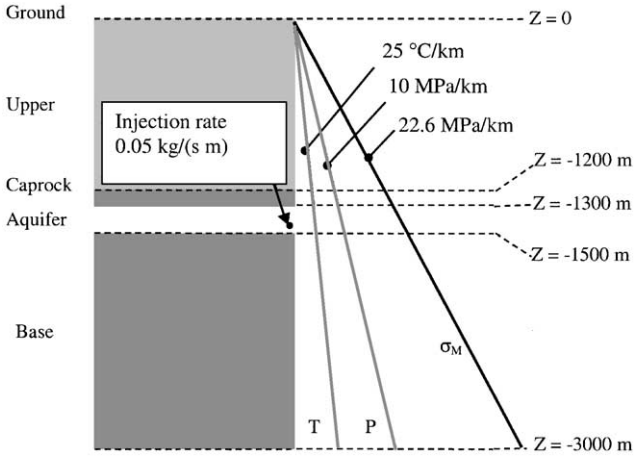

Fig. 4. Geometry and initial conditions for simulation of high pressure CO_2 injection into a brine aquifer. The model is extended laterally far enough to be infinite acting during a 10-year injection period.

The material properties of the injection site are given in Table 1 and correspond to a sandstone aquifer with a caprock of shale. The parameters for the porosity-mean stress and permeability-porosity relationship—ϕ_0, ϕ_r, b, c in Eqs. (19) and (20)—were determined to represent laboratory data by Davis and Davis [18], which shows a one-order-of-magnitude reduction in permeability from zero to 30 MPa effective stress. This TOUGH-FLAC simulation employs a specially developed TOUGH2 module with a realistic fluid-property (PVT) description of brine-CO_2 mixtures for super-critical conditions [26]. It takes into account real gas density and viscosity effects of CO_2, and includes pressure, temperature, and salinity dependence of CO_2 dissolution in the aqueous phase [27].

Fig. 5 presents the calculated injection pressure during a 15-year injection period, with or without consideration of the stress-dependent rock mass permeability. The difference in injection pressure is explained by permeability in the injection zone (in the former case) increasing because of a general reduction in effective stresses. However, the changes in permeability are moderate (less than a factor 2) because of a rather insensitive stress-permeability relationship for the porous sandstone. In this modeling, the injection pressure would exceed the lithostatic pressure (or the minimum compressive principal stress) after about 10 years of injection. At this time, the pressure has propagated a considerable distance inside the brine aquifer, and a pressure change of 1 MPa would be felt more than 15 km away from the injection point. Pressure changes are, however, confined to the injection aquifer and the caprock, while the pressure in the upper aquifer above the caprock remains hydrostatic.

Fig. 6 presents the spreading of the CO_2 fluid within the aquifer/caprock system. The figure shows that the CO_2 has been transported from the injection point up to the bottom of the caprock in about a year, with a lateral spread of about 400 m. At 10 years, the CO_2 has spread

Table 1
Thermal–hydrologic–mechanical properties for simulation of CO_2 disposal in a brine formation

Property	Cap	Aquifer
Young's modulus, E (GPa)	5	5
Poisson's ratio, v (dimensionless)	0.25	0.25
Saturated rock density, ρ_m (kg/m^3)	2260	2260
Zero stress porosity, ϕ_0 (dimensionless)	0.01	0.1
Residual porosity, ϕ_r (dimensionless)	0.009	0.09
Zero stress permeability, k_0 (m^2)	1×10^{-17}	1×10^{-13}
Irreducible gas saturation for Corey's [24] relative permeability function (dimensionless)	0.05	0.05
Irreducible liquid saturation for Corey's [24] relative permeability function (dimensionless)	0.3	0.3
Air-entry pressure for van Genuchten's [25] retention curve (kPa)	3100	19.6
Exponent m for van Genuchten's [25] retention curve	0.457	0.457
Exponent for Eq. (19), a (1/Pa)	5×10^{-8}	5×10^{-8}
Exponent for Eq. (20), c	22.2	22.2
Biot's parameter in Eq. (14), α	1.0	1.0

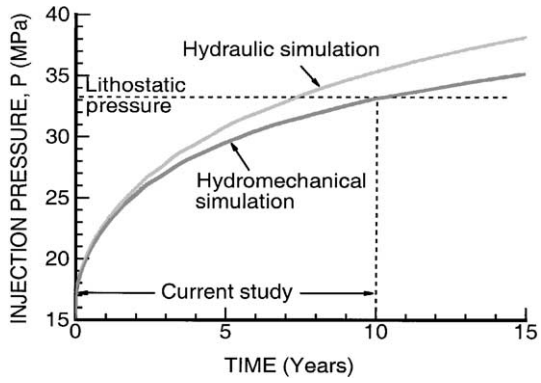

Fig. 5. Calculated injection pressure as a function of time with and without consideration of stress dependent permeability.

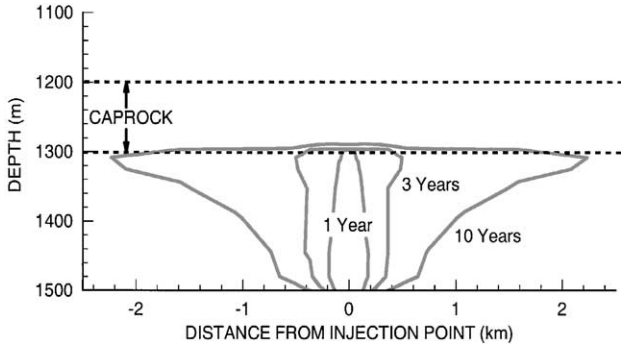

Fig. 6. Spread of the supercritical CO_2 fluid within the brine formation.

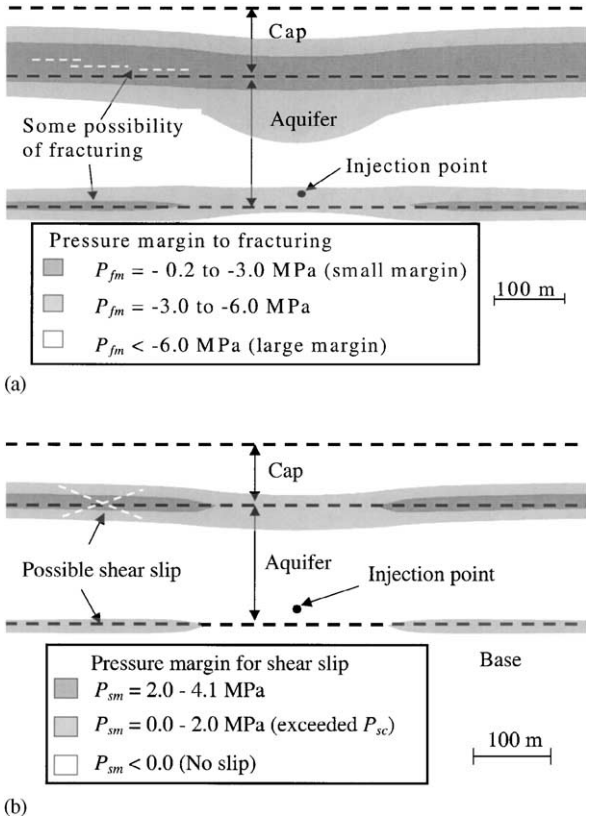

Fig. 7. Pressure margins to (a) hydraulic fracturing and (b) shear slip along pre-existing faults after 10 years of injection. In (a) the pressure margin is the current fluid pressure minus the critical fracturing pressure, i.e. $P_{fm} = P - P_{fc}$ and in (b) the pressure margin is the current fluid pressure minus a critical pressure for slip, i.e $P_{sm} = P - P_{sc}$. The critical pressure for shear slip was calculated using a Coulomb criterion assuming that a fault with zero cohesion and 30° friction angle could exist at any point.

under the cap over 4 km and has penetrated upwards into the caprock by about 10 meters.

The integrity of the caprock could be jeopardized by a mechanical failure, which could occur as a result of hydraulic fracturing or reactivation of pre-existing shear fractures. In this simulation, the potential for hydraulic fracturing and shear-slip reactivation is analyzed and expressed in terms of a pressure margin (Fig. 7). The pressure margin indicates approximately how much further the fluid pressure can be increased without causing rock failure, according to stress criteria for hydraulic fracturing and shear slip. Fig. 7a shows that the pressure margin of hydraulic fracturing is only about 0.1 MPa in the lower part of the caprock, implying an imminent risk of fracturing. More importantly, Fig. 7b shows that the pressure margin for fault slip has been exceeded by 4 MPa. This implies that an unfavorably oriented fault could be reactivated with accompanying micro-seismicity and possible permeability change. However, even if fracturing or fault reactivation would take place in the lower parts of the caprock, the TOUGH-FLAC simulation indicates that it would still likely be contained within the lower portion of the cap.

This application example demonstrates how the specially developed capabilities of the TOUGH2 code for the complex behavior of the supercritical CO_2 could be utilized in a coupled TOUGH-FLAC simulation. These results contribute to identifying the most critical mechanisms for the integrity and long-term stability of a CO_2 injection site. Further studies include effects of a permeable fault [22], heterogeneous reservoir rock, and inelastic aquifer compaction behavior.

7.2. A high temperature nuclear waste repository in unsaturated rock

In this example, the TOUGH-FLAC code is applied to simulate a potential high-temperature (above 100°C) nuclear waste repository in a semi-dry rock formation at Yucca Mountain, Nevada. The simulation domain is defined around a waste-emplacement drift located at 366 meters depth in a multilayered vertical column extending from the ground surface down to the water table (Fig. 8). Laterally, it is bounded on one side by the

vertical symmetry line trough the drift and on the other side by the other vertical line at half-distance between two drifts. Because of a very high fracture density and connectivity in these rock units, a dual-permeability model is used with interacting fractured and matrix continua. In the ambient conditions, almost all the water is held by capillary suction in the matrix (about 95% saturation) near the repository while the fractures are practically dry.

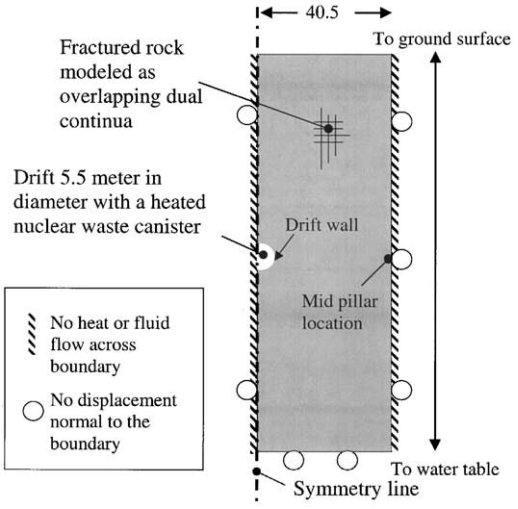

Fig. 8. Geometry and boundary condition for TOUGHFLAC simulation of a high temperature nuclear waste repository.

THM parameters for the rock unit where a repository is assumed to be placed (upper middle nonlithophysal (Tptpmn) of the Topopah Spring Tuff formation at the site) are listed in Table 2. The parameters d and b_{max} that defines the stress-aperture function in Eqs. (28) and (29) were determined according to Rutqvist and Tsang [23] by numerical back-analyses of several field experiments conducted at Yucca Mountain. It was also noted that the fluid pressure in the unsaturated rock system at Yucca Mountain is so low that it could not induce any significant mechanical deformations, and consequently, there is no need to define an effective stress in this case.

In this TOUGH-FLAC simulation, the waste emplacement is designed for a high-temperature or above-boiling case, in which heat input of 1.45 kW/m of drift is applied with a forced ventilation period of 50 years, during which 70% of the decay heat is removed. With such heat input, the calculated temperature rapidly increases and first peaks at around 100°C after about 10 years, followed by a second peak at 200°C a few years after ventilation ceased (Fig. 9). The early time temperature rise induces thermal stresses near the drift with compression of fractures (Fig. 10a). This implies that fracture apertures decrease and consequently the hydraulic permeability is reduced around the drift. After 100 years, permeability has decreased significantly in an area extending hundreds of meters above and below the drift (Fig. 10b). The permeability in the vertical direction changes most because thermal stresses are higher in

Table 2
Thermal–hydrologic–mechanical properties of the Tptpmn rock unit for simulation of a high temperature nuclear waste repository

Type	Property	Value
Hydraulic properties of the fractured continuum	Initial permeability, k_i (m^2)	0.37×10^{-12}
	Initial porosity, ϕ_i (dimensionless)	0.01
	Mean fracture spacing, s (m)	0.23
	Van Genuchten's [25] air-entry pressure (kPa)	1.9
	Van Genuchten's [25] exponent, m (dimensionless)	0.6082
	Residual saturation (dimensionless)	0.01
Hydraulic properties of the matrix continuum	Permeability, k_i (m^2)	0.41×10^{-17}
	Porosity, ϕ_i (dimensionless)	0.11
	Van Genuchten's [25] air-entry pressure (kPa)	258.9
	Van Genuchten's [25] exponent, m (dimensionless)	0.2915
	Residual saturation (dimensionless)	0.19
Thermal properties of the rock mass	Wet thermal conductivity, λ_m (W/m K)	2.33
	Dry thermal conductivity, λ_m (W/m K)	1.56
	Specific Heat, J/(kg K)	948.0
Mechanical properties of the rock mass	Young's modulus, E (GPa)	14.77
	Poisson's ratio, v (dimensionless)	0.21
	Cohesion (MPa)	2.6
	Friction angle (degrees)	57
	Dilation angle (degrees)	29
	Thermal expansion coefficient, β_T (1/°C)	4.14×10^{-6}
	Tensile strength (MPa)	1.54
Hydro-mechanical properties of the fractured continuum	Initial hydraulic aperture for Eq. (9) back-calculated from the initial permeability and spacing using a cubic block conceptual model, b_i (μm)	80.0
	Maximum joint closure for Eq. (9), b_{max} (μm)	541.6
	Exponent for Eq. (9), d (1/Pa)	1.1×10^{-6}

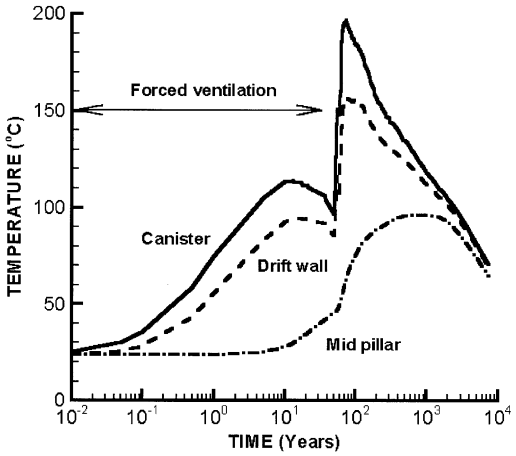

Fig. 9. Temperature evolution at three points on the level of the emplacement drifts. See Fig. 7 for location of points at canister, drift wall and mid pillar.

the horizontal direction due to confinements (no displacement) at the lateral boundaries (Fig. 8).

The TOUGH-FLAC simulation shows that the rapid temperature increase in the early repository time will trigger strongly coupled multiphase transport of moisture and heat, which dries the rock around the tunnel (Fig. 11). As the formation temperature approaches 100°C, matrix pore water boils and vaporizes. Most of the vapor generated moves into the fractures, where it becomes highly mobile and is driven by the gas pressure gradient away from heat source. When vapor reaches cooler rock, it condenses, and the local fracture saturation builds up. Part of the condensate may then imbibe into the matrix, where it is subjected to a strong capillary gradient towards the heat source, giving rise to reflux. However, the strong vapor movement along the thermal gradient dries out the rock mass around the repository drift in a zone with above boiling temperature.

In this example, we could utilize the capabilities of the TOUGH2 code to simulate complex above boiling two-phase flow behavior—for efficiency, this requires special treatment with exchange of primary variables in the numerical solution [4]—and a full THM simulation was achieved through coupling with the FLAC3D code. More long-term results and the impact of these processes on the performance of a potential repository at Yucca Mountain are discussed in Rutqvist and Tsang [23]. Important features of the coupled TOUGH-FLAC code are being validated against field experiments currently underway at Yucca Mountain.

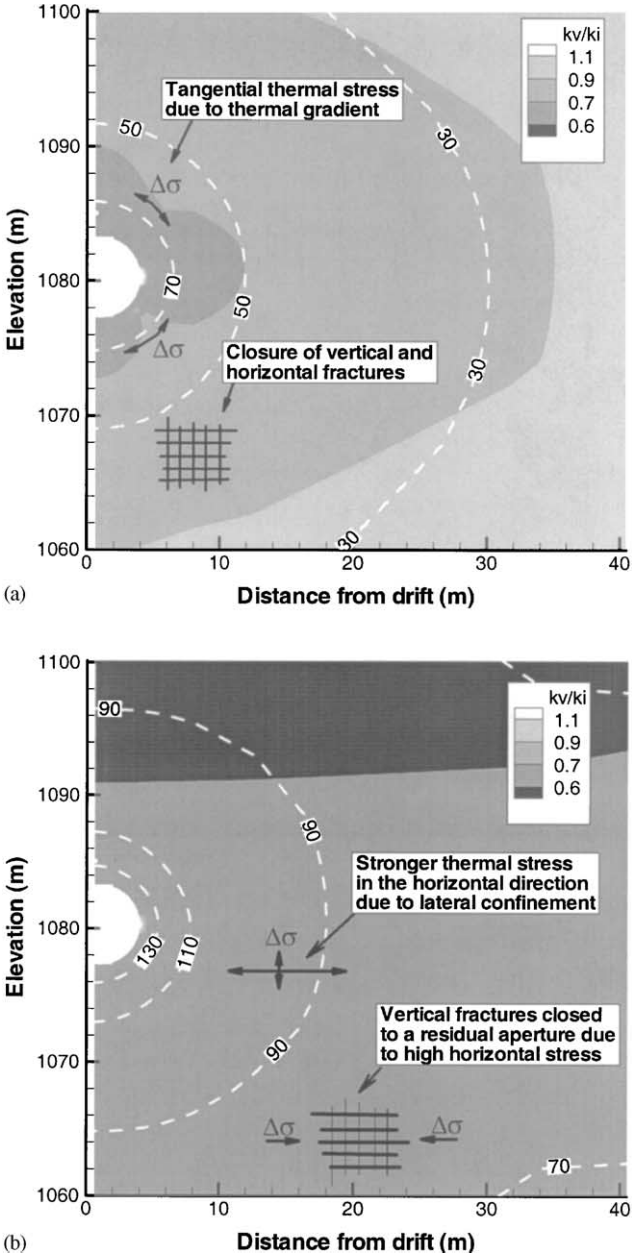

Fig. 10. Calculated contours of temperature and permeability change factor at (a) 10 years and (b) 100 years after emplacement. Dashed lines are isotherms in degree Celsius.

8. Concluding remarks

We have linked two codes—TOUGH2 and FLAC3D—for analysis of coupled THM processes in complex geological media. The codes were linked with modules representing the coupled hydrologic-mechanical behavior for two types of rock masses; sedimentary reservoir rock and highly fractured hard rock. The coupling modules contain nonlinear stress versus permeability functions, which were calibrated against site-specific data. These coupling modules could be exchanged with modules containing any other type of empirical or theoretical hydrologic-mechanical coupling relationship. For example, a complete Biot [11] model or a state surface model [28] could be applied for soil or clay, and effects of shear dilation on fracture

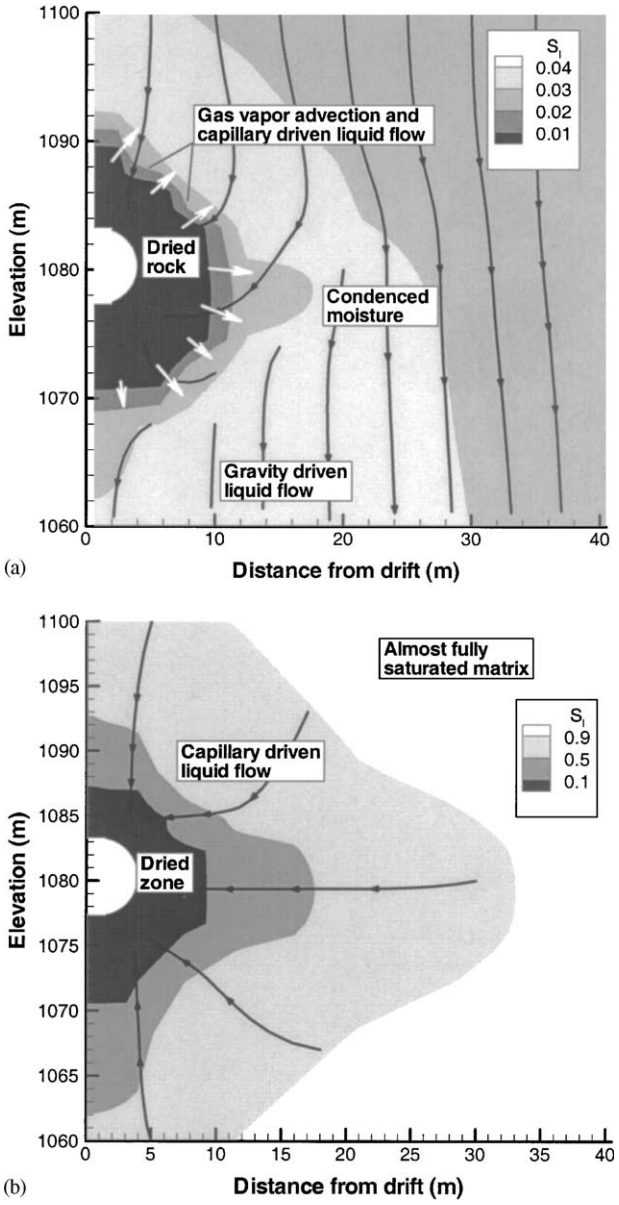

Fig. 11. Liquid water saturation and moisture flow in (a) fractures and (b) matrix at 100 years after emplacement. Solid streamlines reflect the liquid water flow and white arrows are gas vapor flow.

permeability could be added according to Elsworth and Xiang [29]. We have demonstrated the usefulness of linked, sequentially coupled THM analyses for complex problems related to injection and storage of CO_2 in brine aquifer formations and to high temperature nuclear waste disposal in unsaturated rock. In both these examples, the hydromechanical changes are relatively slow, which is most suitable for the sequentially explicit solution. Problems with higher strain rates relative to fluid mobility may require the sequential implicit approach or ultimately a fully implicit coupled approach [30].

Acknowledgements

Reviews by Eric Sonnenthal and Kurt Nihei at Lawrence Berkeley National Laboratory are very much appreciated. This work was jointly supported by the Director, Office of Science, Office of Basic Energy Sciences, Chemical Sciences and Geosciences Division and by the Office of Civilian Radioactive Waste Management, US Department of Energy, through Memorandum Purchase Order EA9013MC5X between Bechtel SAIC Company, LLC and the Ernest Orlando Lawrence Berkeley National Laboratory (Berkeley Lab). The support is provided to Berkeley Lab through the US Department of Energy Contract No. DE-AC03-76SF00098.

References

[1] Tsang C-F. Linking thermal, hydrological, and mechanical processes in fractured rocks. Annu Rev Earth Planet Sci 1999;27:359–84.
[2] Holloway S. An overview of the underground disposal of carbon dioxide. Energy Conversion Manage 1997;38:193–8.
[3] Wawersik WR, Rudnicki W. Terrestrial sequestration of CO_2—an assessment of research needs. Report from invited panelist workshop, May 1997, Department of Energy (DOE) Geosciences Research Program, 1998.
[4] Pruess K. TOUGH2—a general purpose numerical simulator for multiphase fluid and heat flow. Lawrence Berkeley National Laboratory Report LBL-29400, 1991.
[5] Itasca Consulting Group Inc. FLAC-3D Manual: Fast Lagrangian analysis of continua in 3 dimensions–Version 2.0. Itasca Consulting Group Inc., Minnesota, USA, 1997.
[6] Pruess K. Proceedings of the TOUGH Workshop '98. Lawrence Berkeley National Laboratory Report LBNL-41995, Berkeley, CA, 1998.
[7] Xu T, Pruess K. Modeling multiphase non-isothermal fluid flow and reactive geochemical transport in variably saturated fractured rocks 1. Methodol, Am J Sci 2001;301:16–33.
[8] Detournay C, Hart R, editors. FLAC and Numerical Modeling in Geomechanics Proceedings of the International FLAC Symposium on Numerical Modeling in Geomechanics, Minneapolis, 1999. Rotterdam: A. A. Balkema, 1999.
[9] Rutqvist J, Börgesson L, Chijimatsu M, Kobayashi A, Jing L, Nguyen TS, Noorishad J, Tsang C-F. Thermohydromechanics of partially saturated geological media: governing equations and formulation of four finite element models. Int J Rock Mech Min Sci 2001;38:105–27.
[10] Vargaftik NB. Tables of the thermophysical properties of liquids and gases. New York: Wiley, 1975.
[11] Narashimhan TN, Witherspoon PA. An integrated finite difference method for analysis of fluid flow in porous media. Water Resour Res 1976;12:57–64.
[12] Biot MA. General theory of three dimensional consolidation. J Appl Phys 1941;12:155–64.
[13] Bear J, Bachmat Y. Introduction to modeling of transport phenomena in porous media. Netherlands: Kluwer Academic Publisher, 1991.
[14] Bishop AW, Blight GE. Some aspects of effective stress in saturation and partly saturated soil. Geotéchique 1963;13:177–97.
[15] Chen H-Y, Teufel LW. Coupling fluid-flow and geomechanics in dual-porosity modeling of naturally fractured reservoirs. Paper

SPE 38884, Presented at the 1997 SPE Annual Technical Conference and Exhibition, San Antonio, Texas, 5–8 October, 1997.
[16] Walsh JB. Effect of pore pressure and confining pressure on fracture permeability. Int J Rock Mech Min Sci 1981;18:429–35.
[17] Iwano M. Hydromechanical characteristics of a single rock joint. Ph.D. Thesis, Department of Civil and Environmental Engineering, Massachusetts Institute of Technology, 1995.
[18] Davis JP, Davis DK. Stress-dependent permeability: characterization and modeling. Society of Petroleum Engineers, SPE Paper no. 56813, 1999.
[19] Leverett MC. Capillary behavior in porous media. Trans, AIME 1941;142:341–58.
[20] Witherspoon PA, Wang JSY, Iwai K, Gale JE. J.E. Validity of the cubic law for fluid flow in a deformable fracture. Water Resour Res 1980;16:1016–24.
[21] Rutqvist J, Tsang C-F. Stress-permeability functions derived from field tests in fractured rocks, 2002, in preparation.
[22] Rutqvist J, Tsang C-F. A study of caprock hydromechanical changes associated with CO_2 injection into a brine aquifer. Environ Geol, 2002, in press.
[23] Rutqvist J, Tsang CF. Analysis of thermal–hydrologic–mechanical behavior near an emplacement drift at Yucca Mountain. J Contam Hydrol, 2002, accepted for publication.
[24] Corey AT. The interrelation between oil, gas relative permeabilities. Producers Monthly 1954:38–41.
[25] van Genuchten MT. A closed-form equation for predicting the hydraulic conductivity of unsaturated soils. Soil Sci Soc Am J 1980;44:892–8.
[26] Pruess K, Garcia J. Multiphase flow dynamics during CO_2 injection into saline aquifers. Environ Geol, 2002, in press.
[27] Pruess K, Xu T, Apps J, Garcia J. Numerical modeling of aquifer disposal of CO_2. Society of Petroleum Engineers, SPE Paper no 66537, 2001.
[28] Fredlund DG, Rahardjo H. Soil mechanics for unsaturated soil. New York: Wiley, 1993.
[29] Elsworth D, Xiang J. A reduced degree of freedom model for thermal permeability enhancement in blocky rock. Geothermics 1989;18:691–709.
[30] Finite element modelling of three-phase flow in deforming saturated oil reservoirs. Int J Numer Anal Meth Geomech 1993;17:577–89.